PHYSICAL REVIEW D **95,** 023001 (2017)

Cosmic rays in a galactic breeze

Andrew M. Taylor[1,*] and Gwenael Giacinti[2,†]

[1] *Dublin Institute for Advanced Studies, 31 Fitzwilliam Place, Dublin 2, Ireland*
[2] *Max-Planck-Institut für Kernphysik, Saupfercheckweg 1, D-69117 Heidelberg, Germany*

(Received 29 July 2016; revised manuscript received 27 November 2016; published 6 January 2017)

Motivated by the discovery of the nonthermal Fermi bubble features both below and above the Galactic plane, we investigate a scenario in which these bubbles are formed through galacto-centric outflow. Cosmic rays (CR) both diffusing and advecting within a galactic breeze outflow, interacting with the ambient gas present, give rise to γ-ray emission, providing an approximately flat surface brightness profile of this emission, as observed. Applying the same outflow profile further out within the disk, the resultant effects on the observable CR spectral properties are determined. A hardening in the spectra due to the competition of advective and diffusive propagation within a particular energy range is noted, even in the limiting case of equal CR diffusion coefficients in the disk and halo. It is postulated that this hardening effect may relate to the observed hardening feature in the CR spectrum at a rigidity of $\approx$200 GV.

DOI: 10.1103/PhysRevD.95.023001

I. INTRODUCTION

The presence of a galactic wind has considerable impact on an array of topics connected to describing the galactic "halo" environment. With little knowledge about such outer regions of the Galaxy, information provided by nonthermal probes hold the first clues to revealing new information about this galactic frontier.

Over the past few decades, a growing body of evidence has amounted suggesting that our Galactic center (GC) region feeds a wind. Such indications have been provided from a broad observational energy range, from radio HI [1], infrared [2] to X-ray [3]. Infrared observations at larger scales [4] have further indicated that this wind continues out to larger scales and may be responsible for the larger out-of-plane scale structures observed.

More recently, absorption line features in the spectra of distant AGN have been used to probe the gas flow structure [5]. The picture provided by these results indicates the presence of coherent gas flow, consistent with that of an outflow directed away from the galactic plane. Furthermore, recent γ-ray and radio observations [6–9] of the region above and below the GC indicate the presence of extended nonthermal particle populations inside bubble structures which sit above and below the galactic disk. The presence of these cosmic ray (CR) populations are indicative of outflow activity from the GC region. The present picture, therefore, appears to indicate that both hot gas and nonthermal particles are conveyed out from the center of the disk into the halo within a centrally driven galactic wind.

With regards the velocity of the Milky Way's outflow, there are several indicators about this from a host of independent observations. Relatively mild velocities $\sim 300\ \mathrm{km\,s^{-1}}$ are suggested to be present in the outflow region close to the disk ($\sim$1–2 kpc) by the weakness of the X-ray features associated with the bubble edges [6,10–12]. The observation of high velocity clouds in regions consistent with the bubble's location [5], motivate outflow velocities of $\sim 150\ \mathrm{km\,s^{-1}}$ at distances of $\sim$4 kpc and $\sim$9 kpc away of the galactic plane. Further out toward the edges of the bubbles, other indications support velocities $< 100\ \mathrm{km\,s^{-1}}$ in the outflow. Within such a profile scheme, the distortion of the outflow structures seen to high latitudes in radio observations [9] may be related to the motion of the Milky Way towards Andromeda, whose relative velocity is $\sim 50\ \mathrm{km\,s^{-1}}$.

In the following, we consider the secondary signatures that CR embedded in outflows can produce. In Sec. II we adopt simple descriptions for the velocity flow in the outflow and consider the subsequent diffusive-advective motion of CR within it. The generation of secondary signals by these CRs are considered in an effort for simple comparisons with recent observations. In Sec. III, the implications of the presence of galactic driven outflows on the CR detected at Earth are considered. We draw our conclusions from these results in Sec. IV.

II. CR AND γ-RAYS ASSOCIATED WITH A GALACTOCENTRIC OUTFLOW

We describe the propagation of CR within an outflow from the GC region using the diffusion-advection equation. Denoting $\psi_{\mathrm{CR}}(\mathbf{r}, p, t)$ the CR density per unit of particle momentum p, at $\boldsymbol{r}$,

$$\frac{\partial \psi_{\mathrm{CR}}}{\partial t} = \boldsymbol{\nabla} \cdot (\mathcal{D} \boldsymbol{\nabla} \psi_{\mathrm{CR}} - \boldsymbol{V} \psi_{\mathrm{CR}}) + \frac{\partial}{\partial p} \left[\frac{p}{3} (\boldsymbol{\nabla} \cdot \boldsymbol{V}) \psi_{\mathrm{CR}} \right] - \frac{\psi_{\mathrm{CR}}}{\tau_{\mathrm{CR}}} + \mathcal{Q}_{\mathrm{CR}}, \tag{1}$$

---

[*] taylora@cp.dias.ie
[†] giacinti@mpi-hd.mpg.de

where $\mathcal{Q}_{\rm CR}$ is the source term. A diffusion scattering length scale of $\lambda_{10\ \rm GV} = 3\mathcal{D}_{10\ \rm GV}/c = 0.3$ pc is adopted. For CR protons, $\tau_{\rm CR} = \tau_{pp}$ is the energy loss time scale from pp interactions, while for CR nuclei, $\tau_{\rm CR}$ is the interaction time scale.

Motivated by the observations discussed above, we adopt a divergence free outflow velocity profile, whose z-dependence (in a cylindrical coordinate system where the z-axis is perpendicular to the disk) takes the form

$$\boldsymbol{V} \cdot \hat{\mathbf{z}} = v_{\rm max} e^{\frac{1}{2}(1-\frac{d}{z})} \times \frac{2}{1+z/d}, \qquad (2)$$

with $v_{\rm max} = 300\ {\rm km\,s^{-1}}$ and $d = 1$ kpc. For such an outflow velocity profile, a timescale of $\mathcal{O}(100\ {\rm Myr})$ is required in order for the outflow to fill a region beyond the bubbles. As for the source of this outflow, both a past AGN outburst event (see e.g. [13–15]), and a starburst phase or a sustained outflow driven by star formation in the Galactic center (e.g. [16]) have been proposed in the literature. Reference [17] claims that the present velocity data are not conclusive on the type of source responsible for this outflow. Energetically, the starburst driven outflow luminosity is estimated to be $(1\text{–}3) \times 10^{40}\ {\rm erg\,s^{-1}}$ [16]. Although the present level of AGN activity from the Galactic center (of Sgr A*) is considerably below this ($L_{{\rm Sgr}A*} \sim 10^{33}\ {\rm erg\,s^{-1}}$), there is a growing body of evidence that its level in the recent past was significantly higher [18,19]. It therefore presently seems plausible for either energy source to be driving the outflow. In the present work, we prefer to keep the discussion general, adopting instead the specific velocity profile of Eq. (2) as the starting point in our calculations.

Interestingly, such a profile broadly encapsulates the velocity profile of a "breeze" solution for the isothermal outflow problem [20,21]. For such a solution, the wind is launched sufficiently subsonically that it accelerates without becoming transonic, before decelerating after the Bondi radius. The actual launching mechanism of the wind is clearly of particular importance with regards its subsequent velocity evolution with distance. The acceleration profile we adopt is motivated by an isothermal outflow, requiring effective heating of the gas throughout the launching zone.

A range of wind launching and acceleration mechanisms have been considered in the literature: Winds driven by supernovae (see e.g. [22]) and cosmic rays (see e.g. the numerical simulations presented in [23–25]) have both been considered a possibilities. Reference [26] also studied the impact of CRs on the properties of the wind.

In the following, we sudy the impact of outflows on CRs, rather than studying the mechanisms of wind launching and acceleration. To this end, we adopt a specific velocity profile as an input. The breeze profiles we consider, Eq. (2), do not correspond to the wind profiles found in the literature for CR-driven winds, such as in Refs. [27–33]. Nonetheless, our outflow profile is motivated for the Fermi bubbles by observations. Whether such a breeze profile can also describe outflows at larger galactocentric radii is unsure at the present time, but we note that some works, such as Ref. [22], argue that some galaxies can fail to produce successful winds with $dV/dz > 0$ at all z, for example because of the ram pressure of infalling material.

The corresponding gas density profile of our breeze description—Eq. (2), plateaus within the decelerating flow phase. This motivates our naive constant density description for gas in the halo. For breeze outflow scenarios, the peak velocity distance depends on how deep within the gravitational potential the wind is launched and the isothermal temperature of the gas. Adopting motivated numbers for the mass M within the bulge around 1 kpc [34] and the isothermal temperature at the base of the wind [10], the Bondi radius [35] is, $d = 2GM/v_{\rm th}^2 \approx 2(\frac{M}{10^{10}\ M_\odot})(\frac{300\ {\rm eV}}{kT})$ kpc.

We utilize a Monte Carlo approach to solve (1). Our results with this technique have also been compared with those obtained using an explicit differential equation solver, finding excellent agreement in all cases (see Fig. 4 in appendix).

We assume that our source term, $\mathcal{Q}_{\rm CR}$, is constant in time and located at the GC region. The copresence of the resultant accumulated CR with ambient gas gives rise to γ-ray bubble emission through π^0 production generated in pp interactions. This emission may potentially account for the observed γ-rays from the bubbles, as has previously been proposed by others [36].

To determine the level of this emission, the accumulated CR density throughout the outflow region are convolved with the gas target material density in the outflow region. As motivated on theoretical grounds by [37], and on observational grounds by [11], we adopt a constant gas density within the bubble region at the level $3\times10^{-3}\ {\rm cm^{-3}}$. A γ-ray density map and a comparison of the γ-ray bubble-edge profile with Fermi measurement are shown in Fig. 1. For these results, a CR luminosity of $10^{40}\ {\rm erg\,s^{-1}}$ has been adopted for the central source. In this comparison plot, the origin of the diffuse γ-ray emission in the $\theta > 0$ region is assumed purely galactic in origin. Should some component of the emission from this region be extragalactic, however, a subsequent reduction of the Galactic center luminosity or bubble gas density would be required in order to account for such a reduction in required γ-ray emission intensity.

As can be seen from Fig. 1, a flat surface brightness profile for the bubbles is obtained following the assumption that the velocity profile of the bubbles is described by Eq. (2). We note though that in reality a range of velocity profiles can provide such a uniform brightness. See for example [39]. In general, we find that for the case of a constant density ambient medium description, the present γ-ray data can be said to prefer decelerating profiles. Instead, for decreasing gas density profiles, a sharper

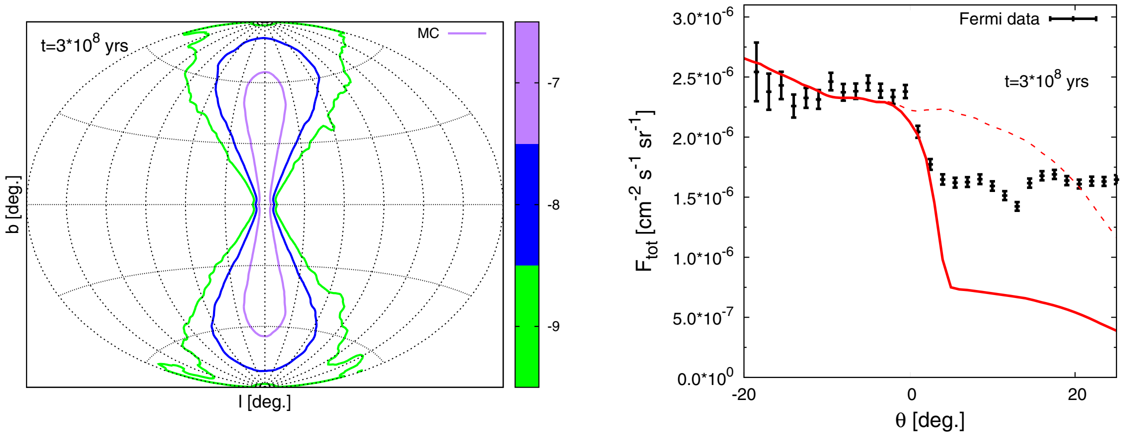

FIG. 1. Left: Contour plots showing $\log_{10}$ of the γ-ray flux surface brightness ($\mathrm{cm}^{-2}\ \mathrm{s}^{-1}\ \mathrm{sr}^{-1}$) from the bubbles following the interaction of CR in the outflow with the gas present. The different line colours indicate the corresponding contour value, whose values are provided in the colour bar in the side-panel. Right: A comparison of the edge of the 1–2 GeV γ-ray bubble from our outflow model with that from the Fermi observation analysis. The angle θ is counted from the edge of the bubble. It is noted that for the energy bin considered, at large θ, further diffuse γ-ray background [38] dominates the observed flux, with the model values sitting below this level in this region. The solid line result adopts a decrease in the gas density at the bubble edge whereas the dashed line result assumes a constant density throughout.

fall-off in the velocity profile, than that adopted in Eq. (2), would be required.

Although the cutoff at the bubble edges is not well described by the simple constant density gas model (see dashed line in Fig. 1), a steeper cutoff in the γ-ray profile can be achieved by a sudden change in the density of the gas at the bubble edge (see solid line), as motivated in certain models [16]. A further motivation for such an origin for the bubble edges comes from a comparison of their morphology as seen in γ-rays [6] and in radio [9]. If GeV protons and electrons respectively give rise to the γ-ray and radio emissions, it would be curious that the electrons extend out to larger latitudes than the protons. Such a difference between γ-ray and radio data morphologies disfavors simple leptonic scenarios for the γ-ray bubbles. Despite such challenges, however, more involved diffuse acceleration models supporting a scenario in which both the radio and γ-ray emission are leptonic in origin are also presently viable [40].

One simple explanation for the difference in latitudinal profiles in the radio and γ-ray emission is that both protons and electrons possess extended distributions, and that the difference in morphology of the secondary emission they produce is dictated by differing distributions of target gas and magnetic fields. A potential association of the astrophysical neutrino events detected by IceCube [41], with the bubbles and beyond [42], allows such a hadronic origin scenario for the γ-rays to be tested in the near future.

III. POTENTIAL IMPLICATIONS FOR CR FLUXES AT EARTH

Out at radii well beyond the GC region, the role played by any advective transport effects is less clear. In order to keep this discussion general, we here explore two extremum cases, namely, a diffusive only transport scenario, and a case in which the inferred GC outflow properties are mirrored at much larger radii.

A. Local contamination of galactocentric outflow

With little evidence that a galactic wind of an appreciable strength exists out at larger galactocentric radii, r, we here impose the extreme assumption that CR propagation in this region ($r > 200$ pc) is purely diffusive. Assuming further that the source is steady on the time scales under consideration [$\mathcal{O}(100\ \mathrm{Myr})$], the subsequent CR density along the disk is expected to follow a $1/r$ dependence within the region where the steady-state has been achieved, with a steeper fall off beyond this point.

Furthermore, TeV γ-ray observations of the GC region by the HESS Cherenkov telescope instrument [43], allow the radial distance at which the inferred CR density drops below its locally measured value to be determined. At an energy of 10 TeV, the CR density at a distance of 100 pc from Sgr A* is ~6 times above the sea level. With a $1/r$ CR density distribution, the transition distance is therefore ~0.6 kpc. However, with a hard CR spectrum observed to be present within this region, this transition distance would be expected to occur at larger radii for higher energy CR. Assuming the CR energy density in the GC region has a spectrum $dN/dE_{\mathrm{CR}} \propto E^{-2.4}$, the ratio of the GC CR energy density to the sea level would be expected to increase as $U_{\mathrm{GC}}/U_{\mathrm{sea}} \propto E_{\mathrm{CR}}^{0.3}$. Consequently, assuming this scaling rule holds, a transition distance of 8 kpc would be reached at an energy of ~20 PeV. This number is derived in the most favorable case of no CR advection in the halo, and, therefore, should be considered as an upper limit for such a

GC contamination. This shows that the GC can, in principle, contribute to the CR flux at PeV energies. However, the observed CR spectrum above the "knee" at these energies is not $\propto E^{-2.4}$, implying the need for a break to exist in the spectrum. Such a solution appears rather *ad hoc*, requiring fine-tuning in order that the Galactic center contributes to the arriving flux without, at the same time, violating spectral shape constraints.

The PeV CR anisotropy direction, however, is compatible with a CR gradient pointing toward the GC. For a CR density $\propto r^{-1}$, the anisotropy amplitude is $\sim \lambda_{1\ \mathrm{PV}}/r_{\mathrm{GC}} \approx 0.6\%$ if $\mathcal{D} \propto E^{1/3}$, which is close to IceCube/IceTop measurements [44]. We note that in a scenario where the PeV CR anisotropy would be due to the GC, the anisotropy below 100 TeV must have a different origin. Indeed, the direction of the CR anisotropy flips by approximately 180° around ≈100 TeV [44], and points in the direction opposite to the GC at low energies. The anisotropy below 100 TeV may, for example, be due to a nearby supernova remnant (SNR). Reference [45] suggested that Vela SNR is a good candidate for shaping the CR anisotropy at Earth below 100 TeV.

B. Local outflow effects

We next study the impact on CR observables of a *local* outflow, whose velocity gradient becomes negative above a given height d in the halo. To our knowledge, the impact of such breeze velocity profiles on the local CR observables has not been presented in the literature yet. While such velocity profiles may not correspond to those expected for CR-driven winds (see e.g. [28,29] where $dV/dz > 0$ at all z), they can be motivated in some models (see e.g. the simulations of Ref. [22] for galaxies failing to produce winds).

As a first approximation, we ignore here any variation of CR sources or propagation parameters in the radial direction from the GC axis. We assume that a one dimensional model is able to encapsulate CR propagation in the halo. Numerically solving the planar diffusion-advection equation in z and E, for any arbitrary profiles of $V(z)$ and $\mathcal{D}(E)$, we coarsely investigate the effect of the advection velocity profile on CR observables. We verified that our code accurately reproduces the expected CR density profiles in the halo for the known cases of V = cst [46] and $V \propto z$ [47], which are constant and decreasing with z, respectively. On the contrary, the $V(z)$ profiles we consider below lead to an increase of CR density above d, decreasing again as $z \to H$ (escape), where H denotes the size of the escape boundary. Physically, the existence of H may correspond to the height at which the magnetic field becomes too weak to confine CR through diffusion. We set $\psi = 0$ at $z = H$ as a boundary condition. We subsequently determine the steady-state distributions for $\psi_{\mathrm{CR}}(z, E)$, for protons, boron and carbon nuclei. For boron and carbon, we denote them as $\psi_{\mathrm{B}}(z, E)$ and $\psi_{\mathrm{C}}(z, E)$.

For the primary source term, we adopt the prescription: $Q_{\mathrm{A}} = 0$ in the halo ($|z| > h = 200$ pc), and $Q_{\mathrm{A}} = f_{\mathrm{A}} Q_{\mathrm{CR}}$ in the disk ($|z| \le h$), where f_{A} is the fraction of species A emitted at the source. For the gas density, we adopt: $n = 0.85\ \mathrm{cm}^{-3}$ at $|z| \le h$, and $n \sim 10^{-3}\ \mathrm{cm}^{-3}$ at $|z| > h$. For clarity, we assume that there are no sources of primary boron.

$\psi_{\mathrm{B,C}}$ satisfy Eq. (1), with the loss terms for C, N, and O, acting as source terms for boron. The source term ($\mathcal{Q}_{\mathrm{CR}}$) in the equation for ψ_{B} is

$$\mathcal{Q}_{\mathrm{B}} = \sum_{\mathrm{Z}} \frac{\psi_{\mathrm{Z}}}{\tau_{\mathrm{Z}\to\mathrm{B}}} = \sum_{\mathrm{Z}} c\sigma_{\mathrm{Z}\to\mathrm{B}} n \psi_{\mathrm{Z}}, \tag{3}$$

where $\tau_{\mathrm{Z}\to\mathrm{B}} = 1/c\sigma_{\mathrm{Z}\to\mathrm{B}} n$ and the contributions from nuclei Z are dominated by C, N, and O. Using the relative abundances of nuclei in the CR flux (see Fig. 6 of [48]), and the production cross-sections $\sigma_{\mathrm{Z}\to\mathrm{B}}$ from [49] and quoted in Table 2 of [48], we rewrite the boron production term as:

$$\mathcal{Q}_{\mathrm{B}} = \frac{\psi_{\mathrm{C}}}{\tau_{\to\mathrm{B}}} = c\sigma_{\to\mathrm{B}} n \psi_{\mathrm{C}}, \tag{4}$$

with $\tau_{\to\mathrm{B}} = 1/c\sigma_{\to\mathrm{B}} n$ and $\sigma_{\to\mathrm{B}} \approx 131$ mb. We take into account destruction of Boron (and similarly for other species) through spallation, with the decay term "$-\psi_{\mathrm{CR}}/\tau_{\mathrm{CR}}$" in Eq. (1) for ψ_{B} set to:

$$-\frac{\psi_{\mathrm{B}}}{\tau_{\mathrm{B}\to}} = -c\sigma_{\mathrm{B}\to} n \psi_{\mathrm{B}}, \tag{5}$$

where $\tau_{\mathrm{B}\to} = 1/c\sigma_{\mathrm{B}\to} n$, and the cross section $\sigma_{\mathrm{B}\to}$ for this process is taken from [50]. We find $\sigma_{\mathrm{B}\to} \approx 250$ mb on pure p target (≈276 mb on 90% p + 10% He). For clarity, we take 250 mb, which is compatible with the value quoted in [51].

We take $H = 25$ kpc, and express $\mathcal{D}$ as $\mathcal{D} = \mathcal{D}_{10\ \mathrm{GV}}(E/(Z \times 10\ \mathrm{GV}))^{\delta}$, setting $\delta = 1/3$ and keeping the same normalization $\mathcal{D}_{10\ \mathrm{GV}}$ as in Sec. II. We have verified that our code reproduces the expected B/C both for the "no wind," and "constant wind" cases. In the latter case, the key parameter is $z_* = \mathcal{D}/V$ (see purple dashed line in Fig. 2), which separates out the distances at which diffusion and advection dominate the particle transport. For low energies, $z_* < H$ and particles advect to the boundary. The B/C ratio shows a quick transition to a constant value at these low energies because $z_* \propto E^{\delta}$. At higher energies, diffusion to the boundary begins to dominate. Since no sudden change of slope is seen in the B/C data, the propagation mode of CR in the energy range sensitive to by present experiments should be predominantly diffusive, i.e., $z_*/H > 1$, demanding an advection wind speed of less than $\mathcal{O}(10\ \mathrm{km\,s^{-1}})$ for $H \sim 10$ kpc, in the case $V = \mathrm{cst}$.

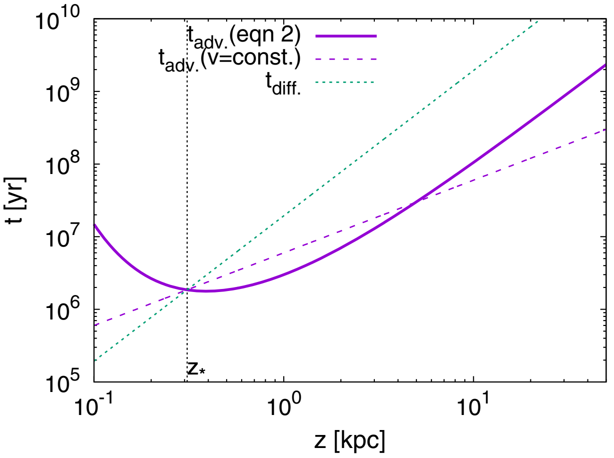

FIG. 2. A comparison of the transport times to different heights, z, above the galactic plane for the both diffusive (t_{diff}) and advective (t_{adv}) transport cases. t_{diff} and z_* are shown here for 10 GV CR. The solid (dashed) line is the advection time out of region z for a velocity profile described by Eq. (2) (for a constant velocity value), and the dotted line is the diffusion time out of the same region.

In general, however, strong winds are not disallowed by the data. Several other wind profiles with $V \neq \mathrm{cst}$ are not ruled out, such as $V(z) \propto z$. We refer to this scenario as a "Bloemen-like" wind [47]. For such a wind, the advection time is independent of z, resulting in $z_* \propto \mathcal{D}^{1/2}$, and the spectral slope tending to $-\alpha - \delta/2$, when $z_* < H$. Thus, the presence of such a wind would lead to a softening spectral index, from $-\alpha - \delta/2$ at low energies, to $-\alpha - \delta$ at high energies. Such a profile, however, would not induce any hardening in the CR spectrum. We show now that hardenings can appear with more complicated wind profiles, and notably with our breeze profile, Eq. (2).

In Fig. 3, we calculate the CR spectrum at $z = 0$ (left-panel), and the B/C ratio (middle-panel) for $V(z)$ from Eq. (2) (red curves), and for a similar profile, namely (2) with $z \to z - 2$ kpc and $V = 0$ at $|z| < 2$ kpc (green curves). Plots of $V(z)$ are shown in the right panel. For reference, we show with thin black lines the "best fit" of the B/C ratio from [48] for $V = 0$. The observational data from AMS-02 for the B/C ratio therefore coincides with this thin black line. We note that we do *not* try to fit the data. Instead, we study, on purpose, caricatural examples in order to explore interesting phenomena allowed by diffusion within a breeze profile, such as the formation of breaks or points of inflection. The parameter values chosen for the breeze profiles presented in Fig. 3 make these features more prominent and more visible than in the data. Fitting the existing data will be investigated in a future work.

Focusing on the shape of the CR spectrum, one can see a point of inflection in each of the curves. In order to interpret these inflection points, a comparison of the advection and diffusion timescales at different energies must be made. In Fig. 2, the advection time for particles at different heights above the galactic plane are shown (solid purple line) for the case corresponding to the red solid line of Fig. 3. Continuing with the assumption that the diffusion coefficient depends only on energy, the curvature of the t_{adv} curve introduces new possibilities as to which of these transport processes dominates. This variety of scenarios, in turn, allows for a broader range of spectral phenomena than the simple leaky box, $V = \mathrm{cst}$ or Bloemen-like wind descriptions. In Fig. 2, the curve for the typical diffusion time t_{diff} (dotted blue line) crosses the advection curve, for sufficiently low energy CR (results shown here for 10 GV CR). This crossing acts as a bottleneck, providing an effective halo height $z_* < H$. At low energies, the outflow then reduces the size of the diffusion "box," within which CR can safely diffuse and return to the observer at $z = 0$, from the full size, H, down to $\sim z_*$. Beyond this distance, advection wins over diffusion, and CR do not come back to $z = 0$. For higher energy CR, however, the diffusion lengths are considerably larger, allowing diffusion to win over advection in the entire halo, and the problem simplifies to a basic leaky-box of size H. With the above

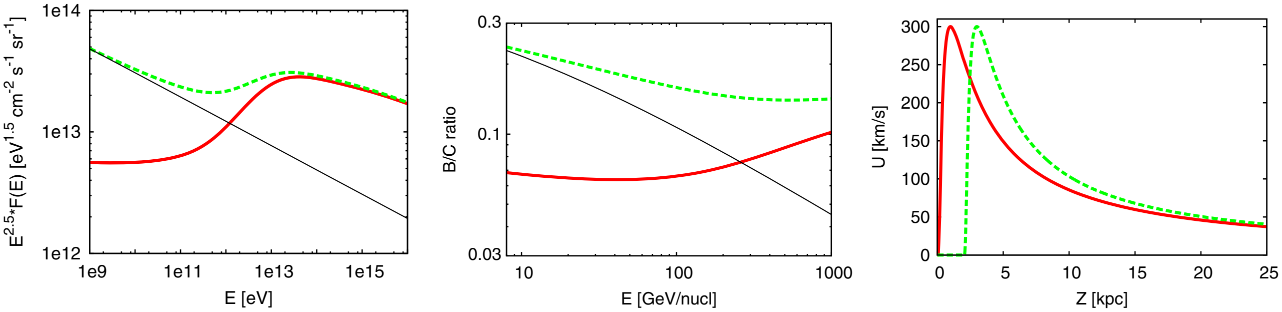

FIG. 3. CR flux (left panel) and B/C ratio (middle) at $z = 0$, for the outflow profiles displayed in the right panel. We do *not* try to fit the data. $\mathcal{D}_{10\,\mathrm{GV}} = 3 \times 10^{28}\ \mathrm{cm}^2\,\mathrm{s}^{-1}$, $\delta = 1/3$, $H = 25$ kpc, $n(z) = 0.85\ \mathrm{cm}^{-3}$ for $|z| \leq h$ and $10^{-3}\ \mathrm{cm}^{-3}$ otherwise, CR spectrum at sources $\propto E^{-2.37}$, and total power injected in CRs at $|z| \leq h$ set to $\approx 3.3 \times 10^{39}\ \mathrm{erg\,pc^{-2}\,yr^{-1}}$. Each scenario is represented by the same line type on each panel. Thin black line for the "best fit" model of [48] with $V = 0$.

parameter values, this happens at energies $E \gtrsim 10^{13\text{–}14}$ eV. As can be seen in Fig. 3 (left panel), the CR spectrum then returns to a power-law of the form $\propto E^{-\alpha-\delta=-2.7}$ at such energies. Below $\sim 10^{12\text{–}13}$ eV, the CR flux is "suppressed."

A more quantitative description of this behavior is provided through the consideration of the change of z_* with diffusion coefficient, described through the relationship, $z_* \propto D^{\beta}$. The $t_{\rm adv}$ curve in Fig. 2 does not vary strongly with z, on $0.2 \lesssim |z|/\mathrm{kpc} \lesssim 2$. Therefore, for low energy CR ($\sim 10^{9\text{–}11}$ eV), $\beta \sim 0.5$. The resultant spectrum is then close to that of a "Bloemen-like" wind, explaining why the spectral index of the red curve in Fig. 3 (left panel) is harder than 2.7 at such energies. At higher energies, β grows larger than 1 and the role of the advection term subsequently quickly turns off. The effective box size abruptly increases from $z_* \lesssim$ a few kpc to H, and the resultant CR spectrum then becomes harder before softening again and matching the spectrum expected for a standard fixed-size diffusion "box," at $E \gtrsim 10^{13\text{–}14}$ eV. Due to this change in box size, the spectrum at high energies is normalized to a larger flux value than the spectrum at low energies. For the green curve, $V = 0$ (i.e. $t_{\rm adv} \to \infty$) at $|z| < 2$ kpc. The corresponding $t_{\rm adv}$ curve would be shifted by $\approx +2$ kpc at low z compared to the curve shown in Fig. 2. In this case, $t_{\rm diff}$ then crosses $t_{\rm adv}$ at a value $z_* \approx 2$ kpc, for CR with $E \lesssim 10^{11}$ eV. In this energy range, the increase of z_* with energy is small compared to 2 kpc. For z slightly greater than 2 kpc, the advection time decreases quickly with z, resulting in β being small ($\ll 1$). The CR spectrum in this low energy region reflects that of the fixed-size diffusion box case, with a box size equal to $\approx$2 kpc. This is why the spectral index of the green curve in Fig. 3 (left panel) tends to 2.7 at low energies.

In summary, the spatially dependent velocity profile we adopt introduces the possibility for a smooth transition from one size diffusion box at low energies, to a larger diffusion box size at higher energies. For some parameter values, it is possible to make the hardening that we found in the CR spectrum coincide better with the one measured at 200 GV by PAMELA, CREAM and AMS-02. Interestingly, if the high-energy softening is left concealed to higher energies ($\gtrsim$3 PeV), one may then explain the 200 GV hardening with the launching of a breeze or wind in the halo, even *without* invoking a change in $\mathcal{D}$ between the disk and the halo. This argument remains valid also for some winds with $dV/dz > 0$ at all z. These data are most sensitive to the accelerating part of the outflow, while those in Sec. II essentially probe the decelerating part of the outflow.

For the same reasons, similar hardenings are expected to appear in the B/C ratio at "intermediate" energies, see middle panel. This is not contradictory with present measurements as long as the hardening is left concealed to higher energies or is hidden within the systematics of the present instruments. Indeed, in connection to the second of these possibilities, it is noted that apparent conflicts in secondary to primary ratios still exist in current data sets (e.g. see Ti/Fe ratio by ATIC-2 [52], HEAO-3-C3 [53], and also their comparison to the B/C ratio [54]).

IV. CONCLUSIONS

We first investigated a scenario in which an advective outflow, emanating from the Galactic center region, carries preaccelerated CR. These CR produce secondary γ-rays via pp interactions on target gas. We have demonstrated that one can reproduce a flat γ-ray surface brightness profile, as is observed for the Fermi bubbles, provided that the outflow decelerates with distance above the Galactic disk. Such a description for the outflow profile is encapsulated by "breeze" solutions of isothermal winds.

Assuming CR propagation beyond the central zone is purely diffusive, it is possible for a non-negligible fraction of CR from the GC region to reach large radii. The contamination under this assumption is energy dependent, and we found that CR from the GC may potentially become the dominant source for the flux observed at Earth, at $\gtrsim$PeV energies. The absence of evidence indicating the onset of a new component in the CR spectrum at these energies, however, place challenges on such a possibility.

Imposing, instead, a wind scenario also out at larger galactocentric radii, we have demonstrated that for the breeze profile (2), an inflection point is introduced into the CR spectrum shape at $z = 0$, as a result of competition between CR advection and diffusion in the halo. We have shown that hardenings can appear in the CR spectrum due to the launching of a breeze or wind in the Milky Way's halo, even without invoking any change in the CR diffusion coefficient value between the disk and halo.

We conclude that a breeze outflow scenario from the Galaxy provides an interesting array of observational signatures able to diagnose its presence. Although presently only motivated from galactocentric outflow observations, the results outlined provide a useful reference for future observations able to disclose its presence at larger radii.

ACKNOWLEDGMENTS

A. T. acknowledges a Schroedinger fellowship at DIAS. The authors would like to thank Ruizhi Yang for helpful discussions about the Fermi data and results. Insightful discussions on the role played by the outflow with Roland Crocker are also gratefully acknowledged.

APPENDIX A: GALACTIC CENTER OUTFLOW SIMULATIONS

As a cross-check on the solutions to Eq. (1) obtained, a comparison of the results obtained from both the

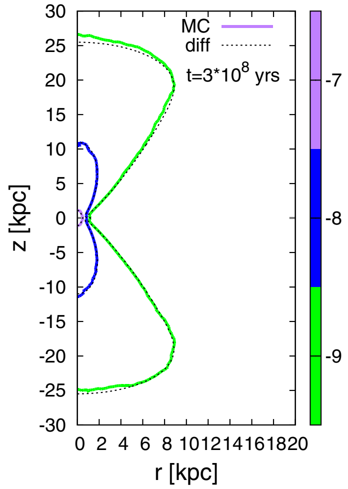

FIG. 4. A comparison plot showing the $\log_{10}$ cosmic ray density contours (cm^{-3}) obtained using both the Monte Carlo and differential equation solver methods. “MC” refers to the Monte Carlo result and “diff” to that from the differential equation solver. The different line colors indicate the corresponding contour value obtained from the MC method, whose values are provided in the color bar in the side-panel. The dashed lines are the results from the differential equation solution.

Monte Carlo and differential equation solver methods are shown in Fig. 4. As is evident from this plot, very good agreement is found between the two methods. Note the boundary and system setup conditions for this result were the same as that for the main paper text. Namely, a continuous source term, Q_{CR} was located in the central region, a constant diffusion coefficient ($\mathcal{D}_{10\,\mathrm{GV}}$) was assumed, and an advective outflow described by (2) was adopted.

APPENDIX B: SIMULATIONS FOR OUTFLOWS AT LARGER GALACTOCENTRIC RADII

We show here some of the code verifications relating to the calculations presented in Sec. III B.

We verified that our code can reproduce the expected CR fluxes and spectra as functions of z for the $V(z) = 0$, $V(z) = \mathrm{cst}$ and $V(z) \propto z$ wind profiles. As an example, we show in Fig. 5 (left panel) our calculations of the normalized CR spectra multiplied by $E^{2.1}$, $E^{2.1}\mathrm{N}(E)/\mathrm{N}(E = 10^4\ \mathrm{GeV}, z = 0)$, at $z = 0$ (black solid line) and $z = 10$ kpc (green solid line), using the parameters of Fig. 1 of Ref. [47] for $V_0 = 10\ \mathrm{km\,s^{-1}\,kpc^{-1}}$, where

$$V(z) = 3V_0 z. \tag{B1}$$

The parameters are: $H = 20\,\mathrm{kpc}$, $\mathcal{D}_{10\mathrm{GV}} \simeq 4.0\times10^{29}\,\mathrm{cm^2\,s^{-1}}$, $\delta = 0.6$, and the spectral index at the sources is $\alpha = 2.1$. Good agreement is found between this result and its equivalent in Fig. 1 of Ref. [47].

Concerning the calculation of the boron-to-carbon ratio, we verified, amongst other tests, that our code can reproduce the results for the benchmark fit presented in Fig. 3 of Ref. [48]. The parameters of this benchmark fit are $V(z) = 0$, $H = 4$ kpc, $\mathcal{D}_{10\ \mathrm{GV}} \simeq 4.8\times10^{28}\ \mathrm{cm^2\,s^{-1}}$, and $\delta = 0.44$. The results from our code are plotted in the right panel of Fig. 5 (green solid line). The agreement with Fig. 3 of Ref. [48] is good.

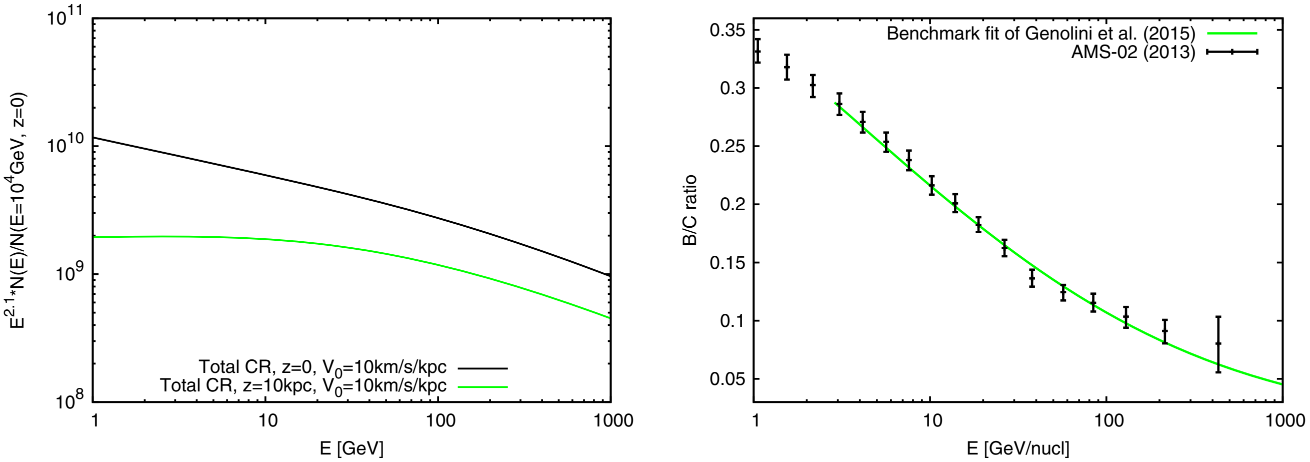

FIG. 5. Left panel: Calculation of the CR spectrum $E^{2.1}\mathrm{N}(E)/\mathrm{N}(E = 10^4\ \mathrm{GeV}, z = 0)$ at $z = 0$ (black solid line) and $z = 10$ kpc (green solid line) with our code, using the parameters of Fig. 1 of Ref. [47] for $V_0 = 10\ \mathrm{km\,s^{-1}\,kpc^{-1}}$, where $V(z) = 3V_0 z$. $H = 20$ kpc, $\mathcal{D}_{10\ \mathrm{GV}} \simeq 4.0\times10^{29}\ \mathrm{cm^2\,s^{-1}}$, $\delta = 0.6$, and $\alpha = 2.1$. Right panel: Calculation of the boron-to-carbon ratio with our code, using the parameters of the “benchmark fit” of Ref. [48] (green solid line) and compared with AMS data [54] (black errorbars). The parameters of the benchmark fit of [48] are: $V(z) = 0$, $H = 4$ kpc, $\mathcal{D}_{10\ \mathrm{GV}} \simeq 4.8\times10^{28}\ \mathrm{cm^2\,s^{-1}}$, and $\delta = 0.44$.

[1] F. J. Lockman, The H I halo in the inner galaxy, Astrophys. J. **283**, 90 (1984).
[2] M. Morris and E. Serbyn, The galactic center environment, Annu. Rev. Astron. Astrophys. **34**, 645 (1996).
[3] L. X. Cheng, M. Leventhal, D. M. Smith, W. R. Purcell, J. Tueller, A. Connors, D. Dixon, R. L. Kinzer, and J. G. Skibo, A Maximum entropy map of the 511 keV positron annihilation line emission distribution near the galactic center, Astrophys. J. **481**, L43 (1997).
[4] J. Bland-Hawthorn and M. Cohen, The large-scale bipolar wind in the galactic center, Astrophys. J. **582**, 246 (2003).
[5] B. A. Keeney, C. W. Danforth, J. T. Stocke, S. V. Penton, J. M. Shull, and K. R. Sembach, Does the Milky Way produce a nuclear galactic wind?, Astrophys. J. **646**, 951 (2006).
[6] M. Su, T. R. Slatyer, and D. P. Finkbeiner, Giant gamma-ray bubbles from Fermi-LAT: AGN activity or bipolar galactic wind?, Astrophys. J. **724**, 1044 (2010).
[7] R. z. Yang, F. Aharonian, and R. Crocker, The Fermi bubbles revisited, Astron. Astrophys. **567**, A19 (2014).
[8] M. Ackermann *et al.* (Fermi-LAT Collaboration), The spectrum and morphology of the Fermi bubbles, Astrophys. J. **793**, 64 (2014).
[9] E. Carretti, R. M. Crocker, L. Staveley-Smith, M. Haverkorn, C. Purcell, B. M. Gaensler, G. Bernardi, M. J. Kesteven, and S. Poppi, Giant magnetized outflows from the centre of the Milky Way, Nature (London) **493**, 66 (2013).
[10] J. Kataoka, M. Tahara, T. Totani, Y. Sofue, L. Stawarz, Y. Takahashi, Y. Takeuchi, H. Tsunemi *et al.*, Suzaku observations of the diffuse x-ray emission across the fermi bubbles' edges, Astrophys. J. **779**, 57 (2013).
[11] T. Fang and X. Jiang, High resolution X-Ray spectroscopy of the local hot gas along the 3C 273 sightline, Astrophys. J. **785**, L24 (2014).
[12] A. J. Fox *et al.*, Probing the fermi bubbles in ultraviolet absorption: A spectroscopic signature of the milky way's biconical nuclear outflow, Astrophys. J. **799**, L7 (2015).
[13] F. Guo and W. G. Mathews, The Fermi bubbles. I. Possible evidence for recent AGN jet activity in the Galaxy, Astrophys. J. **756**, 181 (2012).
[14] F. Guo, W. G. Mathews, G. Dobler, and S. P. Oh, The Fermi bubbles II: The potential roles of viscosity and cosmic ray diffusion in jet models, Astrophys. J. **756**, 182 (2012).
[15] M. V. Barkov and V. Bosch-Ramon, Formation of large-scale magnetic structures associated with the Fermi bubbles, Astron. Astrophys. **565**, A65 (2014).
[16] R. M. Crocker, G. V. Bicknell, A. M. Taylor, and E. Carretti, A unified model of the Fermi bubbles, microwave haze, and polarized radio lobes: Reverse shocks in the Galactic center's giant outflows, Astrophys. J. **808**, 107 (2015).
[17] K. C. Sarkar, B. B. Nath, and P. Sharma, Supernovae vs AGN: Clues to the origin of Fermi Bubbles from OVIII/OVII line ratio, arXiv:1610.00719.
[18] R. Terrier, G. Ponti, G. Bélanger, A. Decourchelle, V. Tatischeff, A. Goldwurm, G. Trap, M. R. Morris, and R. Warwick, Fading hard X-ray emission from the Galactic Centre molecular cloud Sgr B2, Astrophys. J. **719**, 143 (2010).
[19] G. Ponti, R. Terrier, A. Goldwurm, G. Belanger, and G. Trap, Discovery of a superluminal Fe K echo at the Galactic Center: The glorious past of Sgr A* preserved by molecular clouds, Astrophys. J. **714**, 732 (2010).
[20] J. W. Chamberlain, On the Existence of slow solutions in coronal hydrodynamics, Astrophys. J. **141**, 320 (1965).
[21] E. N. Parker, Dynamical properties of stellar coronas and stellar winds, IV. the separate existence of subsonic and supersonic solutions, Astrophys. J. **141**, 1463 (1965).
[22] Y. Dubois and R. Teyssier, On the onset of galactic winds in quiescent star forming galaxies, Astron. Astrophys. **477**, 79 (2008).
[23] T. Peters, P. Girichidis, A. Gatto, T. Naab, S. Walch, R. Wünsch, S. C. O. Glover, P. C. Clark, R. S. Klessen, and Christian Baczynski, Impact of supernova and cosmic-ray driving on the surface brightness of the galactic halo in soft X-rays, Astrophys. J. **813**, L27 (2015).
[24] M. Hanasz, H. Lesch, T. Naab, A. Gawryszczak, K. Kowalik, and D. Wltaski, Cosmic rays can drive strong outflows from gas-rich high-redshift disk galaxies, Astrophys. J. **777**, L38 (2013).
[25] P. Girichidis, T. Naab, S. Walch, M. Hanasz, M.-M. Mac Low, J. P. Ostriker, A. Gatto, T. Peters, R. Wünsch, and S. C. O. Glover, Launching cosmic-ray-driven outflows from the magnetized interstellar medium, Astrophys. J. **816**, L19 (2016).
[26] C. M. Simpson, R. Pakmor, F. Marinacci, C. Pfrommer, V. Springel, S. C. O. Glover, P. C. Clark, and R. J. Smith, The role of cosmic ray pressure in accelerating galactic outflows, Astrophys. J. **827**, L29 (2016).
[27] V. S. Ptuskin, H. J. Völk, V. N. Zirakashvili, and D. Breitschwerdt, Transport of relativistic nucleons in a galactic wind driven by cosmic rays, Astron. Astrophys. **321**, 434 (1997).
[28] D. Breitschwerdt, V. A. Dogiel, and H. J. Völk, The gradient of diffuse gamma-ray emission in the galaxy, Astron. Astrophys. **385**, 216 (2002).
[29] S. Recchia, P. Blasi, and G. Morlino, Cosmic ray driven Galactic winds, Mon. Not. R. Astron. Soc. **462**, 4227 (2016).
[30] A. Socrates, S. W. Davis, and E. Ramirez-Ruiz, The Eddington limit in cosmic rays: An explanation for the observed faintness of starbursting galaxies, Astrophys. J. **687**, 202 (2008).
[31] J. E. Everett, E. G. Zweibel, R. A. Benjamin, D. McCammon, L. Rocks, and J. S. Gallagher, The Milky Way's kiloparsec scale wind: A hybrid cosmic-ray and thermally driven outflow, Astrophys. J. **674**, 258 (2008).
[32] S. Samui, K. Subramanian, and R. Srianand, Cosmic ray driven outflows from high redshift galaxies, Mon. Not. R. Astron. Soc. **402**, 2778 (2010).
[33] E. A. Dorfi and D. Breitschwerdt, Time-dependent galactic winds I. Structure and evolution of galactic outflows accompanied by cosmic ray acceleration, Astron. Astrophys. **540**, A77 (2012).
[34] E. Dwek, R. G. Arendt, M. G. Hauser, T. Kelsall, C. M. Lisse, S. H. Moseley, R. F. Silverberg, T. J. Sodroski, and J. L. Weiland, Morphology, near-infrared luminosity, and mass of the Galactic bulge from COBE DIRBE observations, Astrophys. J. **445**, 716 (1995).
[35] H. Bondi, On spherically symmetrical accretion, Mon. Not. R. Astron. Soc. **112**, 195 (1952).

[36] R. M. Crocker and F. Aharonian, Fermi Bubbles: Giant, Multibillion-Year-Old Reservoirs of Galactic Center Cosmic Rays, Phys. Rev. Lett. **106**, 101102 (2011).

[37] R. Feldmann, D. Hooper, and N. Y. Gnedin, Circum-galactic gas and the isotropic gamma ray background, Astrophys. J. **763**, 21 (2013).

[38] A. A. Abdo *et al.* (Fermi-LAT Collaboration), The Spectrum of the Isotropic Diffuse Gamma-Ray Emission Derived From First-Year Fermi Large Area Telescope Data, Phys. Rev. Lett. **104**, 101101 (2010).

[39] K. C. Sarkar, B. B. Nath, and P. Sharma, Multiwavelength features of Fermi bubbles as signatures of a galactic wind, Mon. Not. R. Astron. Soc. **453**, 3827 (2015).

[40] P. Mertsch and S. Sarkar, Fermi Gamma-Ray 'Bubbles' from Stochastic Acceleration of Electrons, Phys. Rev. Lett. **107**, 091101 (2011).

[41] M. G. Aartsen *et al.* (IceCube Collaboration), Evidence for high-energy extraterrestrial neutrinos at the IceCube detector, Science **342**, 1242856 (2013).

[42] A. M. Taylor, S. Gabici, and F. Aharonian, Galactic halo origin of the neutrinos detected by IceCube, Phys. Rev. D **89**, 103003 (2014).

[43] A. Abramowski *et al.* (HESS Collaboration), Acceleration of petaelectronvolt protons in the Galactic Centre, Nature (London) **531**, 476 (2016).

[44] M. G. Aartsen *et al.* (IceCube Collaboration), Anisotropy in cosmic-ray arrival directions in the Southern Hemisphere with six years of data from the IceCube Detector, Astrophys. J. **826**, 220 (2016).

[45] M. Ahlers, Deciphering the Dipole Anisotropy of Galactic Cosmic Rays, Phys. Rev. Lett. **117**, 151103 (2016).

[46] A. J. Owens and J. R. Jokipii, Cosmic rays in a dynamical halo. I—Age and matter traversal distributions and anisotropy for nuclei. II—Electrons, Astrophys. J. **215**, 677 (1977).

[47] J. B. G. M. Bloemen, V. A. Dogiel, V. L. Dorman, and V. S. Ptuskin, Galactic diffusion and wind models of cosmic-ray transport. I—Insight from CR composition studies and gamma-ray observations, Astron. Astrophys. **267**, 372 (1993).

[48] Y. Genolini, A. Putze, P. Salati, and P. D. Serpico, Theoretical uncertainties in extracting cosmic-ray diffusion parameters: the boron-to-carbon ratio, Astron. Astrophys. **580**, A9 (2015).

[49] W. R. Webber, A. Soutoul, J. C. Kish, and J. M. Rockstroh, Updated formula for calculating partial cross sections for nuclear reactions of nuclei with $Z \leq 28$ and $E > 150$ MeV Nucleon^{-1} in Hydrogen Targets, Astrophys. J. Suppl. Ser. **144**, 153 (2003).

[50] R. K. Tripathi, F. A. Cucinotta, and J. W. Wilson, Accurate universal parameterization of absorption cross sections III – light systems, Nucl. Instrum. Methods Phys. Res., Sect. B **155**, 349 (1999).

[51] M. S. Longair, *High Energy Astrophysics* (Cambridge University Press, Cambridge, 2011), 3rd ed.

[52] V. I. Zatsepin *et al.*, Energy dependence of Ti/Fe ratio in the Galactic cosmic rays measured by the ATIC-2 experiment, Astron. Lett. **35**, 338 (2009).

[53] V. Vylet, J. C. Waddington, R. W. Binns, L. T. Garrard, H. M. Israel, J. Klarmann, and M. Metzger, in *Proceedings of the 21st International Cosmic Ray Conference*, University of Adelaide, Northfield, South Australia, 1990, Volume 3.

[54] AMS Collaboration, in *Proceedings of the 33rd ICRC, Rio de Janeiro, Brazil, 2013* (Brazilian Journal of Physics, Rio de Janeiro, 2013).